

## Article

# Cementitious Backfill with Partial Replacement of Cu-Rich Mine Tailings by Sand: Rheological, Mechanical and Microstructural Properties

Nihat Utku Guner<sup>1,2</sup>, Erol Yilmaz<sup>1,3,\*</sup> , Muhammet Sari<sup>1,2,3</sup>  and Tugrul Kasap<sup>1,2</sup> 

<sup>1</sup> Geotechnical, Waste Management and Backfill Laboratory, Recep Tayyip Erdogan University, Fener, Rize TR53100, Türkiye

<sup>2</sup> Institute of Graduate Studies, Recep Tayyip Erdogan University, Fener, Rize TR53100, Türkiye

<sup>3</sup> Department of Civil Engineering, Geotechnical Division, Recep Tayyip Erdogan University, Fener, Rize TR53100, Türkiye

\* Correspondence: erol.yilmaz@erdogan.edu.tr

**Abstract:** The thinning of tailings gradation during ore processing leads to a sizeable fall in the strength of cementitious paste backfill (CPB), increases operational risks, and encourages researchers to use alternative economic products. This study aims to increase the strength performance by improving CPB's gradation while cutting costs and reducing the sum of the binder employed per unit volume. An evolution of the slump/strength/structural properties of sand-substituted CPBs was explored experimentally. Samples were made with a fixed cement content (7 wt.%), diverse tailings/sand fractions (e.g., 100/0, 90/10, 80/20, 70/30, and 50/50), and diverse solid contents (e.g., 72 and 76 wt.%). After curing for 3–56 days, several experiments, such as slump, uniaxial compressive strength (UCS), mercury intrusion porosimetry (MIP), and scanning electron microscopy (SEM), were undertaken for the filling samples. The results demonstrate that adding sand to the backfill greatly increases CPB's strength (up to 99%), but the replacement rate of sand was limited to 30% due to its segregation effect. Microstructural tests reveal that CPB's void volume decreases as the added amount of sand increases. To sum up, it was concluded that calcareous sand made a major contribution to the filling strength, incorporating the effects of enhancing the fill gradation's readjustment and reducing the sum of cement being used in the unit volume for CPB manufacturing.

**Keywords:** sand; cementitious backfill; slump; strength acquisition; porosity; microstructure



**Citation:** Guner, N.U.; Yilmaz, E.; Sari, M.; Kasap, T. Cementitious Backfill with Partial Replacement of Cu-Rich Mine Tailings by Sand: Rheological, Mechanical and Microstructural Properties. *Minerals* **2023**, *13*, 437. <https://doi.org/10.3390/min13030437>

Academic Editors: Yanli Huang and Junmeng Li

Received: 24 February 2023

Revised: 10 March 2023

Accepted: 17 March 2023

Published: 18 March 2023



**Copyright:** © 2023 by the authors. Licensee MDPI, Basel, Switzerland. This article is an open access article distributed under the terms and conditions of the Creative Commons Attribution (CC BY) license (<https://creativecommons.org/licenses/by/4.0/>).

## 1. Introduction

In recent years, huge tailings were generated while extracting ore from the mining industry to create major economic (e.g., high capital/operating costs), social (e.g., strict governmental rules and public awareness), and environmental (e.g., acid mine drainage AMD) problems [1–3]. Considering this situation, the research and development of effective tailings disposal methods or technologies have become inevitable today [4,5]. One of the most innovative tailings discarding ways is to employ a cementitious paste backfill (CPB) for modern mines [6–8]. CPB significantly reduces the environmental risks of AMD and heavy metals while eliminating the requirement for surface tailings disposal areas [9–11]. In addition, CPB economically helps to provide an efficient cost-ground support tool for underground structures [12–14]. It is a composite mixture of tailings (65–85 wt.% solids), cement (by a dosage of 2–8 wt.%), and mixing water (e.g., process, lake, and tap) [15,16]. Sometimes, different mineral (e.g., slag and fly ash) and chemical (e.g., plasticizer) additives can be added to CPB mixtures [17,18]. The physicochemical/mineralogical characteristics of tailings directly govern the quality/behavior of the manufactured CPB mixtures [19,20]. However, the reduction in particle size for the extraction of low-grade ores during milling adversely affects tailings' physical properties (e.g., lower size of particles) [21–23]. CPB

with finer tailings particles leads to lower uniaxial compressive strength values than that of coarser tailings particles [24–26]. As a creative solution to low aggregate material in the tailings, sand with relatively coarse particles can be the remedy for high backfill performance [27–29]. Inert materials such as sand can modify the gradation of finer tailings by bringing them to an appropriate grain size distribution [30,31].

The particle size of the sand gained by crushing/grinding operations greatly affects properties such as the void ratio and fluidity of cemented mixtures [32,33]. Well-graded sand has a lower void ratio which contributes positively to the final strength of cemented mixtures [34,35]. Similarly, the thinning of the particle size of sand increases its corresponding surface area and ensures that the grains gain a smooth structure [36]. In addition, coarser and angular sands increase the friction between particles, which has a remarkable factor in the development of the filling strength [37,38]. However, the excessive use of coarser sands in the mixture increases voids between particles (it needs high cement dosages to reach equal strengths for CPB) and can cause several operational problems (e.g., segregation, blockages, and failure) during pipeline transportation [39–41]. Hence, the amount of sand used in the mixture needs to be adjusted carefully to avoid these problems. In addition to the physical and rheological properties of sand, its chemical/mineralogical properties also affect the overall performance of CPB mixtures [42,43].

Many researchers have addressed this issue by investigating them from different aspects. Yang et al. [44] presented a flow experiment to guess the density drops in the pipeline of CPB prepared with cemented Gobi sand and tailings and found that their model could efficiently envisage the gravity drop in Bingham liquids exhibiting a laminar movement in the pipe. Zhou et al. [45] conducted an experimental study using OPC/fly ash as cement and sand as aggregate for backfilling in comparison to conventional CPB without fly ash and sand additives. They found that CPB specimens had a large bleeding rate and early (0.2–0.4 MPa) and that the late (7–9 MPa) compressive strengths of CPB were quite low. Sun et al. [46] explored the strength gaining of Aeolian sand-based filling mixes with different aspects (e.g., sand, fly ash, water, cement) at times that elapsed from 1 day to 28 days. They found that CPB samples prepared with Aeolian sand showed a rise in the strengths for the first 7-days of curing, but the strengths of CPB gradually decreased with increasing sand content (e.g., 70%) for 28 days of curing. They investigated the microstructural changes of 28-day cured fills consisting of tailings/sand mixtures and stated that adding a 5 wt.% cement to CPB mixture resulted in a significant reduction (five folds) in the pore size. Deng et al. [47] indicated that the strength of CPB consisting of waste rock/fly ash/lime/cement (as coarse aggregate/fine aggregate/activator/binder) improved with a large growth in solids of up to 75%, but a decrease in water content reduced workability clearly.

Although there are many studies on the use of diverse additives as a tailing's replacement material for CPB, the use of sand as an alternative product is still a key issue that requires detailed research [48–50]. This paper aims to investigate the performance of sand when used as a substitute for tailings in CPB by considering different aspects: two different solid contents (72 and 76 wt.%), three different tailings/sand ratios (90/10, 70/30, and 50/50 wt.%), and CEM-I 42.5R (7 wt.%). Some rheological (slump), mechanical (uniaxial compressive strength UCS), and microstructural (scanning electron microscopy SEM, X-Ray fluorescence spectroscopy XRF and mercury intrusion porosimetry MIP) experiments were undertaken for the backfills prepared with crushed sand. This paper also includes some useful thoughts about the trials achieved and the key outcomes when sand was added CPBs.

## 2. Materials and Methods

### 2.1. Materials

#### 2.1.1. Sieved Sand

The sand obtained from a quarry around the mine under the test was employed for making mine backfill specimens. Figure 1 indicates the sand's particle size distribution

(PSD) curve. It is apparent that the sand’s D50 value was found to be 1.12 mm while its maximum particle size was under 3.35 mm. This sieve size reflects the allowable maximum particle size within transportable paste backfill mixtures into underground stopes via a pipeline. The tested sand was well graded as the coefficient of curvature,  $C_c$ , varied from 1 to 3 (in this case, this value was computed as 1.35) while the coefficient of uniformity,  $C_u$ , was higher than 6 (in this case, this value was computed as 13.1). Table 1 also lists some physical properties of the sand used. The sand’s specific gravity  $GS$  and surface area  $SS$  values were found to be 2.63 and  $0.71 \text{ m}^2/\text{g}$ , respectively.

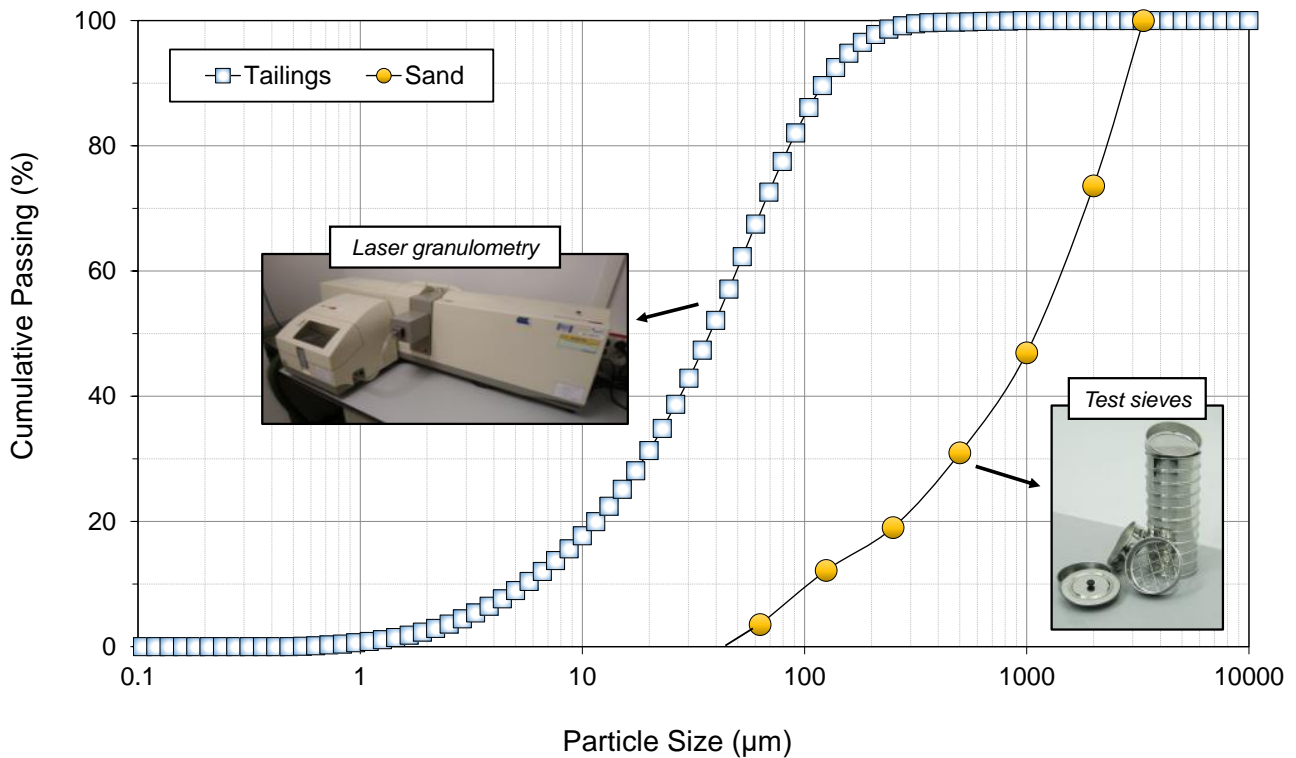


Figure 1. Cumulative PSD curves of Cu-rich tailings and sand.

Table 1. A summary of basic physical features of tailings, sand, and cement.

Physical Parameters	Tailings	Sand	Cement
Specific gravity, $GS$	3.55	2.63	3.12
Specific surface area, $SS, \text{m}^2/\text{g}$	2.89	0.71	0.43
$D_{10}, \mu\text{m}$	5.96	113	4.62
$D_{30}, \mu\text{m}$	24.1	476	12.8
$D_{50}, \mu\text{m}$	43.6	1122	23.1
$D_{60}, \mu\text{m}$	60	1483	32.3
$D_{90}, \mu\text{m}$	132	2541	69
$C_u$ , Coefficient of uniformity ( $D_{60}/D_{10}$ )	10.1	13.1	6.99
$C_c$ , Coefficient of curvature ( $(D_{30}^2)/(D_{60} \times D_{10})$ )	1.62	1.35	1.10

The sand’s composition was chemically analyzed by the PANalytical/Epsilon 5 energy dispersion XRF spectrometry. Table 2 lists the sand’s chemical composition. One can see clearly that the major oxide within the sand was calcium oxide ( $\text{CaO}$ : 55.6%), while the minor phases within the sand were silicon dioxide ( $\text{SiO}_2$ : 1.85%) and aluminum oxide ( $\text{Al}_2\text{O}_3$ : 1.51%). Note that the loss-on-ignition (LOI) was relatively high (41.28%).

**Table 2.** Oxide analyses of tailings/sand/cement materials.

Oxide Analysis	Tailings (%)	Sand (%)	Cement (%)
Fe <sub>2</sub> O <sub>3</sub>	41.8	0.44	3.13
Mn <sub>3</sub> O <sub>4</sub>	0.93	0.02	0.03
BaO	0.02	0.01	0.09
TiO <sub>2</sub>	0.34	0.03	0.20
CaO	4.25	55.6	64.5
K <sub>2</sub> O	0.29	0.09	0.79
SO <sub>3</sub>	0.39	0.75	3.53
P <sub>2</sub> O <sub>5</sub>	0.05	0.01	0.03
SrO	0.01	0.01	0.08
SiO <sub>2</sub>	26.5	1.85	16.9
Al <sub>2</sub> O <sub>3</sub>	7.11	1.51	5.81
MgO	1.65	0.59	1.22
Na <sub>2</sub> O	0.04	0.02	0.39
LOI	20.1	41.28	3.90

### 2.1.2. Copper Tailings

The Cu-rich mine tailings were employed for paste backfill manufacturing. The PSD analysis of the studied tailings sample was measured by a Malvern Mastersizer 2000 laser granulometer (able to measure particles up to 2 mm). Figure 1 indicates the tailings' particle size distribution (PSD) curve. One can infer that the tailings' fines content ( $-20\ \mu\text{m}$ ) was 28.8% (it can be classified as coarse-sized tailings when compared to a standard material content ranging from 15% to 35%, based on Landriault's tailings sorting method). GS and SS values for the tailings sample were found to be 3.55 and 2.89 m<sup>2</sup>/g, respectively. Table 1 also indicates some basic physical properties of the tailings.

The tailings' chemistry was also analyzed by XRF spectrometry. Table 2 indicates the tailings' oxide analysis result. One can visibly infer that iron oxide (Fe<sub>2</sub>O<sub>3</sub>: 41.8%) and silicon dioxide (SiO<sub>2</sub>: 26.5%) were redetected as major oxide phases. In addition, copper grades within processing tailings varied between 0.13 and 1.18 mg/L.

### 2.1.3. Cement and Mixing Water

In this study, CEM I 42.5R was adopted as the cement. Table 2 tabulates the oxide analysis results of cement. CaO and SiO<sub>2</sub> contents were detected as 64.5% and 16.9%, respectively. Table 1 also indicates the cement's key characteristics. The cement's specific gravity and specific surface were 3.12 and 0.43 m<sup>2</sup>/g, respectively. To thoroughly blend the key ingredients (tailings/sand/cement), only tap water was used as mixing water.

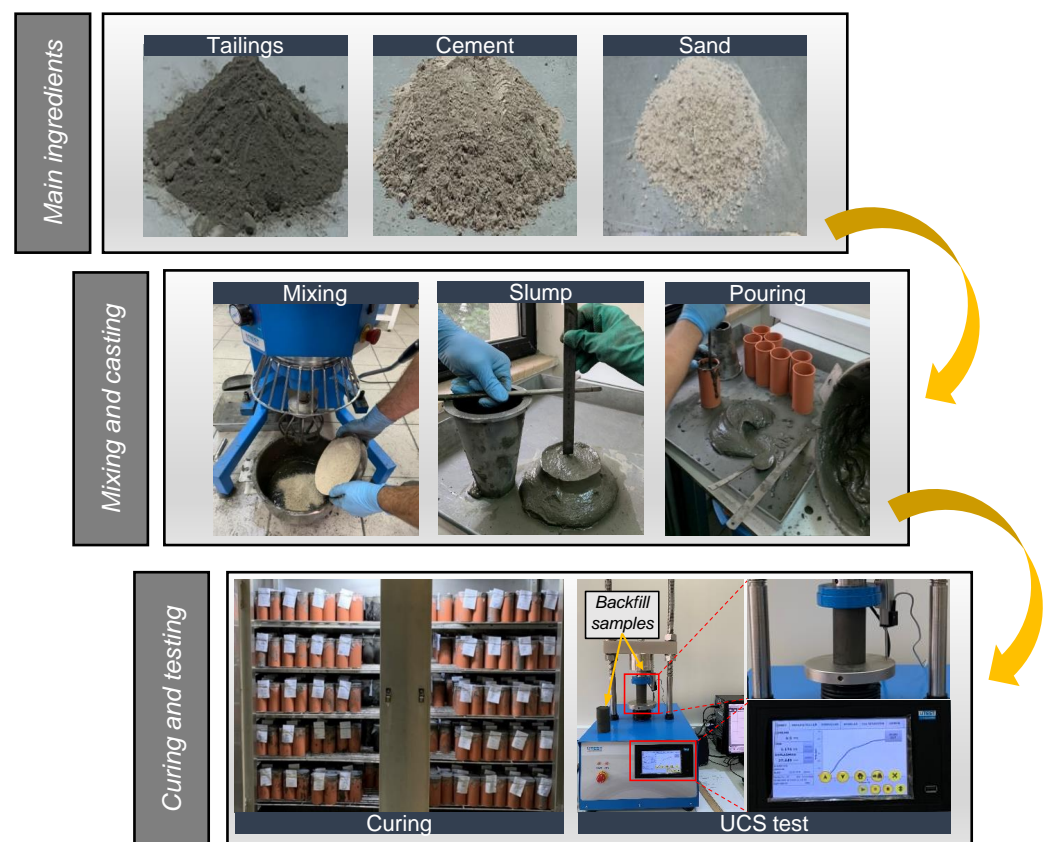
## 2.2. CPB Manufacturing

CPBs were prepared in the lab, respecting the recipes that were pre-determined. Table 3 indicates the CPB recipe design. According to the selected cement content (7 wt.%), the addition of sand to CPB (72/76 wt.% solid contents) was adjusted to 0% (control), 10%, 20%, 30%, and 50% of the total tailings mass, respectively. The backfill amounts were first weighed with the help of precision scales. Tailings and water were blended in a 10-L capacity UTEST mixer for 3 min. Ordinary Portland Cement (OPC) and sand were then added and mixed for another 4 min.

To achieve the wanted slump for CPB samples, the total time required was determined as 7 min. Each mixture was then compressed 25 times with the aid of a steel rod and placed in the mini-slump cone in increments of one third to obtain the appropriate consistency. As in the slump tests, the mixture was placed in one-third volume increments into a cylindrical plastic mold (D × H: 5 × 10 cm) and compacted as indicated above. To denote underground mining conditions, a curing cabinet was maintained at a temperature of 20 °C and 85% humidity. The samples were placed in a cabinet and kept there until the pre-determined curing times. Figure 2 shows the sample preparation process.

**Table 3.** CPB recipe design (CT: copper tailings).

Notation	Curing Time (Days)	Solid Content (wt.%)	Slump (cm)	OPC (wt.%)	Tailings (wt.%)	Sand (wt.%)
CT100-72	3, 14, 28, 56	72	25	7	100	-
CT100-76	3, 14, 28, 56	76	21	7	100	-
CT90-S10-72	3, 14, 28, 56	72	25	7	90	10
CT90-S10-76	3, 14, 28, 56	76	21	7	90	10
CT80-S20-72	3, 14, 28, 56	72	25	7	80	20
CT80-S20-76	3, 14, 28, 56	76	21	7	80	20
CT70-S30-76	3, 14, 28, 56	72	25	7	70	30
CT70-S30-76	3, 14, 28, 56	76	21	7	70	30
CT50-S50-A	3, 14, 28, 56	72	25	7	50	50
CT50-S50-B	3, 14, 28, 56	76	21	7	50	50

**Figure 2.** Specimen preparation steps.

### 2.3. Methods

#### 2.3.1. Miniature Slump Cone Tests

The slump of backfill samples with or without sand was measured by a miniature slump cone (15 cm height; Figure 2) according to the ASTM C143 code. Instead of a standard slump cone (30 cm height) which was typically employed as a measure of concrete flowability, tests using a miniature slump cone required small volumes of backfill materials [51,52]. Experience displays that standard and miniature slump cones represent a strong relationship. Overall, the miniature slump cone provided half of the slump measured by a standard slump cone. The slump determined by a miniature slump cone was measured as 50 mm, while the slump value determined by a standard slump cone was measured as 100 mm. The target slump values of the paste backfill mixtures were determined as 250 mm and 210 mm for a given solid content of 72 wt.% and 76 wt.%, respectively.

### 2.3.2. Mechanical Strength Tests

For UCS tests, an auto-controlled UTEST Multiplex Universal device (capacity: 50 kN; displacement: 1 mm/min) was employed on cylinder-shaped specimens ( $D \times H: 5 \times 10$  cm). Before starting the test, the upper and lower surfaces of CPB specimens to be positioned between low and top metal circles were leveled. The strength value of backfilling was acquired by averaging three UCS test results.

### 2.3.3. SEM Observations

After UCS testing, the effect of inert sand on microstructural changes in CPB was explored by JEOL JSM-6510 type scanning electron microscopy. The microscope's key parameters were 10–30 kV acceleration voltage, 2000 times magnification, and 3 nm resolution. Before the SEM analyses, CPB pieces were put in alcohol first and were then furnace dehydrated at 50 °C for 5 days to wholly stop the backfill's cement hydration process. Note that SEM analyses were conducted at an acceleration voltage of 25 keV with 0.9 nA current emission.

### 2.3.4. MIP Measurements

After the UCS test, the effect of sand on the fill's microstructure was explored by a Quantachrome PoreMaster PM60-type mercury intrusion porosimetry. The porosimeter's key parameters were 3–210 kPa low pressure, 0.21–410 MPa high pressure, and 0.003  $\mu\text{m}$  pore diameter. Before MIP tests, 2–5 g cylindrical samples were oven-dried first and then subjected to low/high pressures sequentially. Note that MIP tests were conducted at a Hg body volume of 70%, a 130° contact angle, and 0.485 N/m surface tension. CPB's porosities were acquired by averaging three MIP test results.

## 3. Results and Discussion

### 3.1. Sand Effect on CPB's Strength Property

Figure 3 demonstrates the strength evolution of CPB samples when prepared with diverse tailings/sand ratios. The average strengths of the backfill samples generally increased depending on the sand replacement rates.

The average strengths of the reference samples (CT100-72 and CT100-76) for different curing times were found to be 0.35, 0.58, 0.78, and 0.88 MPa, as well as 0.43, 0.80, 1.00, and 1.15 MPa, respectively. The mean strengths of the CT90-S10-72 (25 cm slump) and CT90-S10-76 (21 cm slump) samples varied in the range of 0.50–1.07 MPa and 0.64–1.28 MPa, respectively. In cases of CT50-S50-72 and CT50-S50-76, where the amount of sand used instead of tailings was the highest, the strength ranges reached 0.65–1.17 MPa, and 0.83–1.42 MPa, respectively. When CPB mixtures prepared with different tailings/sand ratios at a 72 wt.% solid content were considered, backfill strengths increased in the ranges of 42.5%–89.0%, 38.9%–60.9%, 20.6%–38.5%, and 21.9%–40.4% for 3, 14, 28, and 56 days, respectively. For the 76 wt.% solid content, backfill strengths at these curing times increased in the range of 47.7%–99.2%, 21.4%–54.1%, 11.4%–32.8%, and 11.6%–33.4%, respectively.

The main reason behind these increases in strengths is that sand improved the particle size distribution of tailings [53]. In addition, sand samples containing high amounts of CaO can interact with cement and contribute to the creation of a suitable pH environment for hydration, increasing the pH to ideal levels [54,55]. Considering both the increase in strength and the rheological properties, the ideal tailings/sand ratio was determined as 70/30. It has been observed that if the amount of sand used was more than this ratio, it caused segregation, which reduced CPB's workability. The grain structure, shape, and size of the sand to be selected for CPB manufacturing should be well explored, as this may cause extra friction losses during the delivery of CPB via a pipeline, including the wear on the elbows and the slowing down or even stopping of operations.

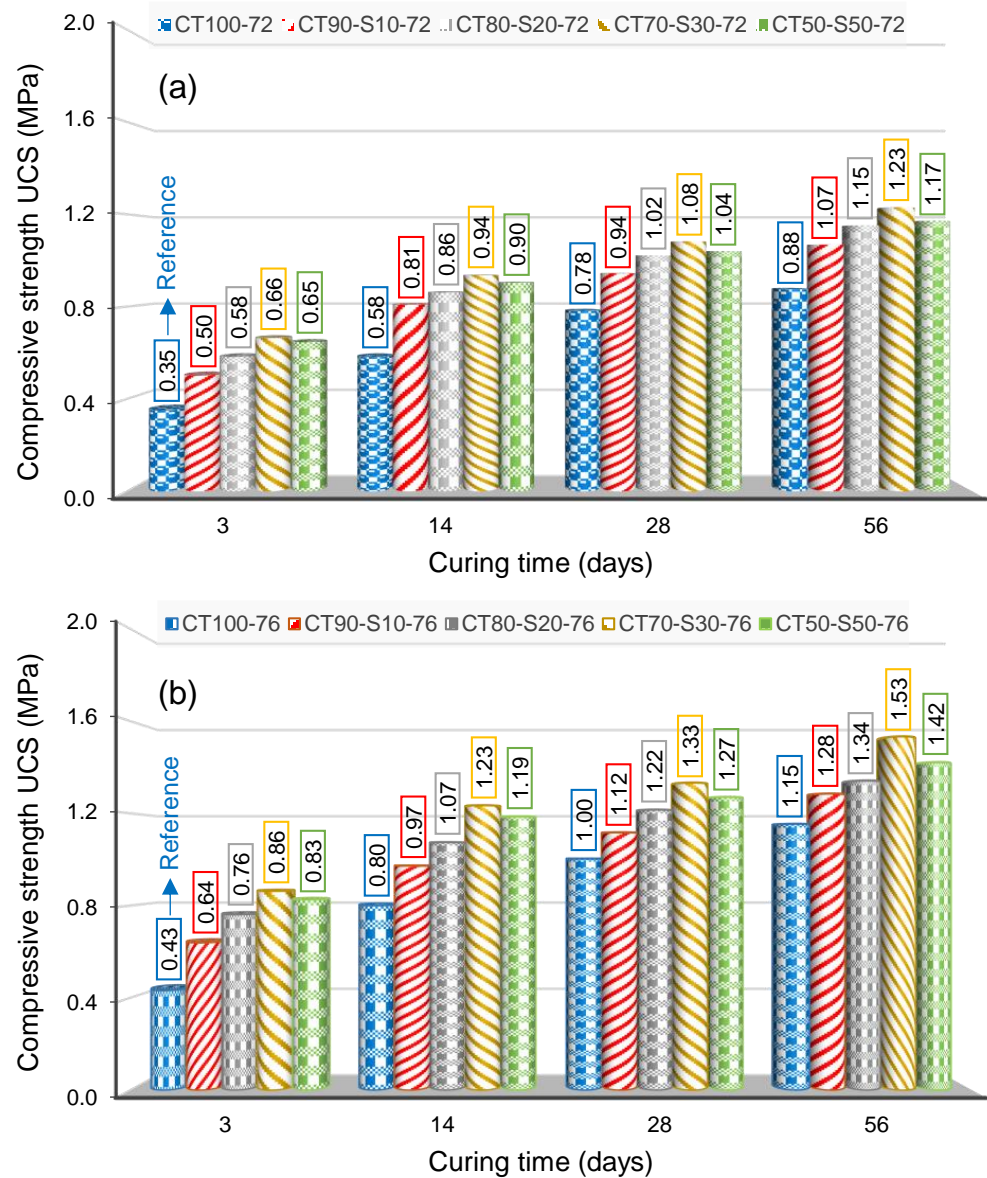


**Figure 3.** The compressive strengths of CPB with different sand ratios: (a) 72 wt.% and (b) 76 wt.%.

### 3.2. Influence of Tailings-To-Sand Rate on Backfill Failure

The stress–strain curves of 56-day cured filling specimens with different tailings/sand ratios are given in Figure 4. Stress–strain curves can be evaluated in four steps: (i) pore solidity step, (ii) elastic distortion step, (iii) plastic yield step, and (iv) rupture-breakage step [56,57].

Cementitious filling specimens that were tested at the first stage demonstrated many voids due to grains of sand. Therefore, from the first stress implemented, the micro-voids of cementitious paste backfill began to close, and a concave stress–strain curve was shaped. In the second step, cementitious paste backfill specimens entered the elastic deformation stage, and the strain was augmented with increasing stress. Therefore, the curve developed a traditional line, and micro-cracks began to form in the backfilling. The modulus of elasticity of backfill with diverse sand replacement ranks was acquired. As can be seen from Figure 4, in 76 wt.%, solid content as the sand substitution rank was augmented from 0% to 50%, the rupture-breakage values for the filling specimens were higher than the 72 wt.% solid content. This meant that the addition of sand improved the confrontation of backfilling to distortion.

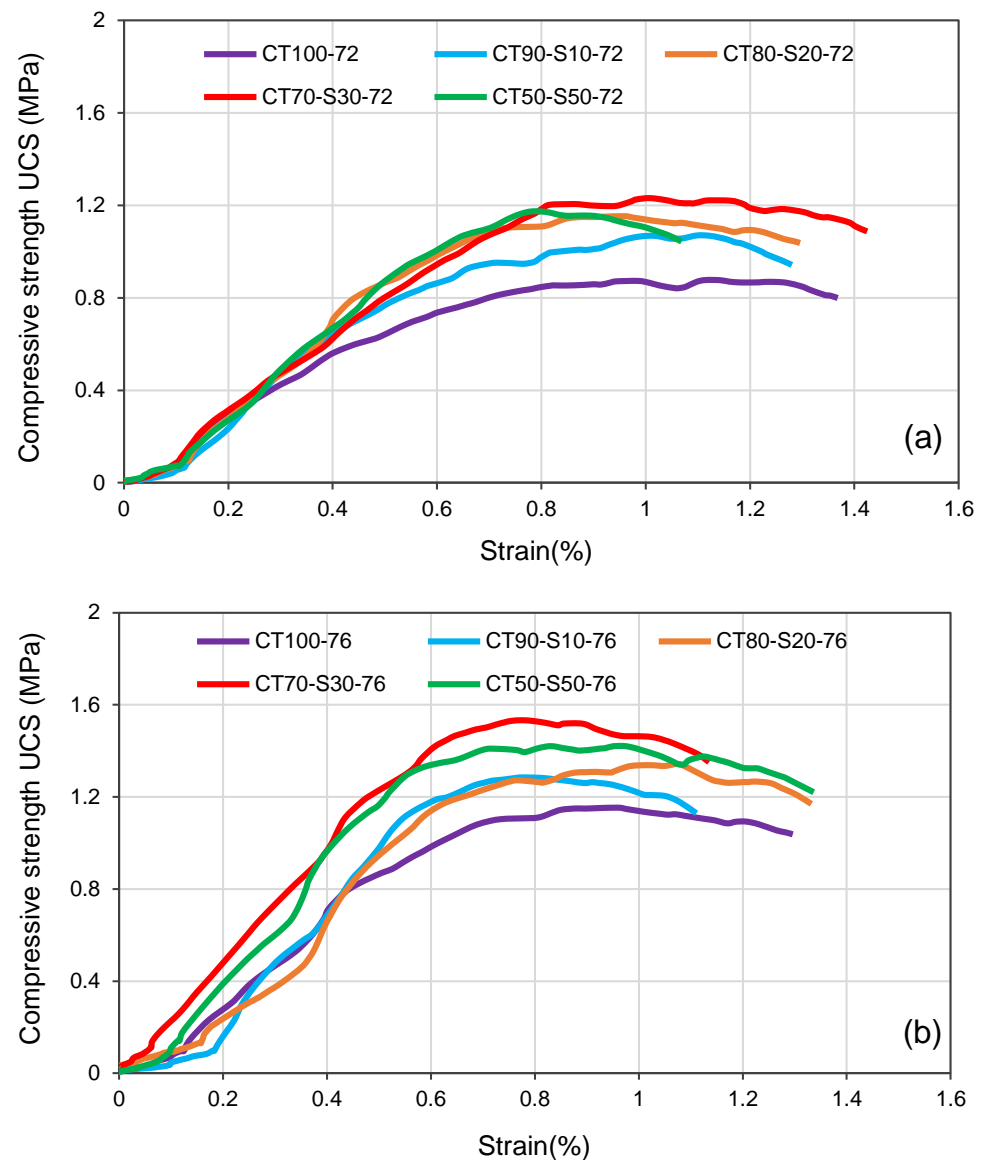


**Figure 4.** Stress–strain curves of 56-day cured fills with (a) 72 wt.% and (b) 76 wt.% solids.

In the third step, elastic distortion rotated into plastic distortion. The inner pores/cracks of the filling samples progressively extended, stress–strain curves became convex, and gradually reached their highest mechanical strength values. Significant differences occurred in the peak stresses, with reductions in the strains corresponding to the maximum stresses that occurred as the sand substitution increased. It was determined that the unit deformation values corresponding to the peak stress at 72 wt.% and 76 wt.% solid contents were between 0.78% and 1.11% and between 0.77% and 1.08%.

In the last step, after the specimens extended the peak, as the stress amplified, the micro-cracks of the samples merged, and fracture planes were formed. As the loading continued, the pressure progressively reduced, and all specimens had a residual strength once breaking. The residual strength of cementitious paste backfills with sand appeared to be slightly higher than that of CPB without sand. Almost all the samples tested showed strong brittleness after reaching the peak stress. Since filling specimens reinforced with sand still had a high bearing capacity even after collapse compared to filling specimens reinforced with no sand, this demonstrates that sand can be used as an additive material to increase the safety of underground operations.

### 3.3. MIP Analysis of Filling Specimens

Figures 5 and 6 indicate the cumulative MIP results of filling specimens on different curing days. It is quite apparent that for a certain mix recipe, CPB's total porosity decreased with an increased curing time. For all curing times at 72–76 wt.% solid contents, the total porosity values of the backfill control samples were found to be in the ranges of 50.4%–52.2% and 47.2%–49.2%, respectively. Similarly, for different tailings/sand ratios, these values were found to be in the ranges of 49.0%–51.9% and 44.0%–48.3%, respectively. The well-graded sand used in filling specimen mixtures provided lower porosity compared to the reference samples.

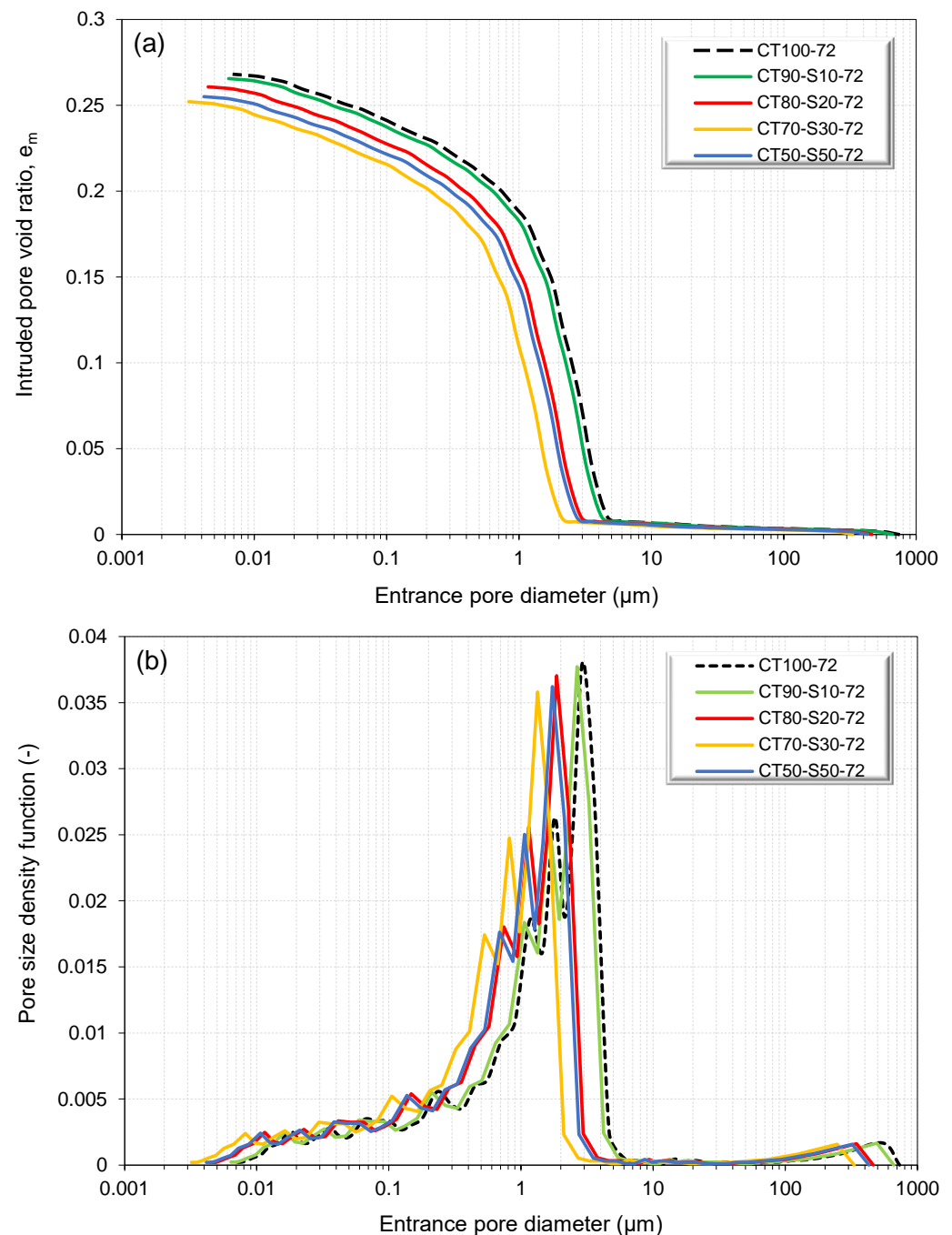


**Figure 5.** MIP results of 72 wt.% solid fill specimens: (a) cumulative; (b) incremental curves.

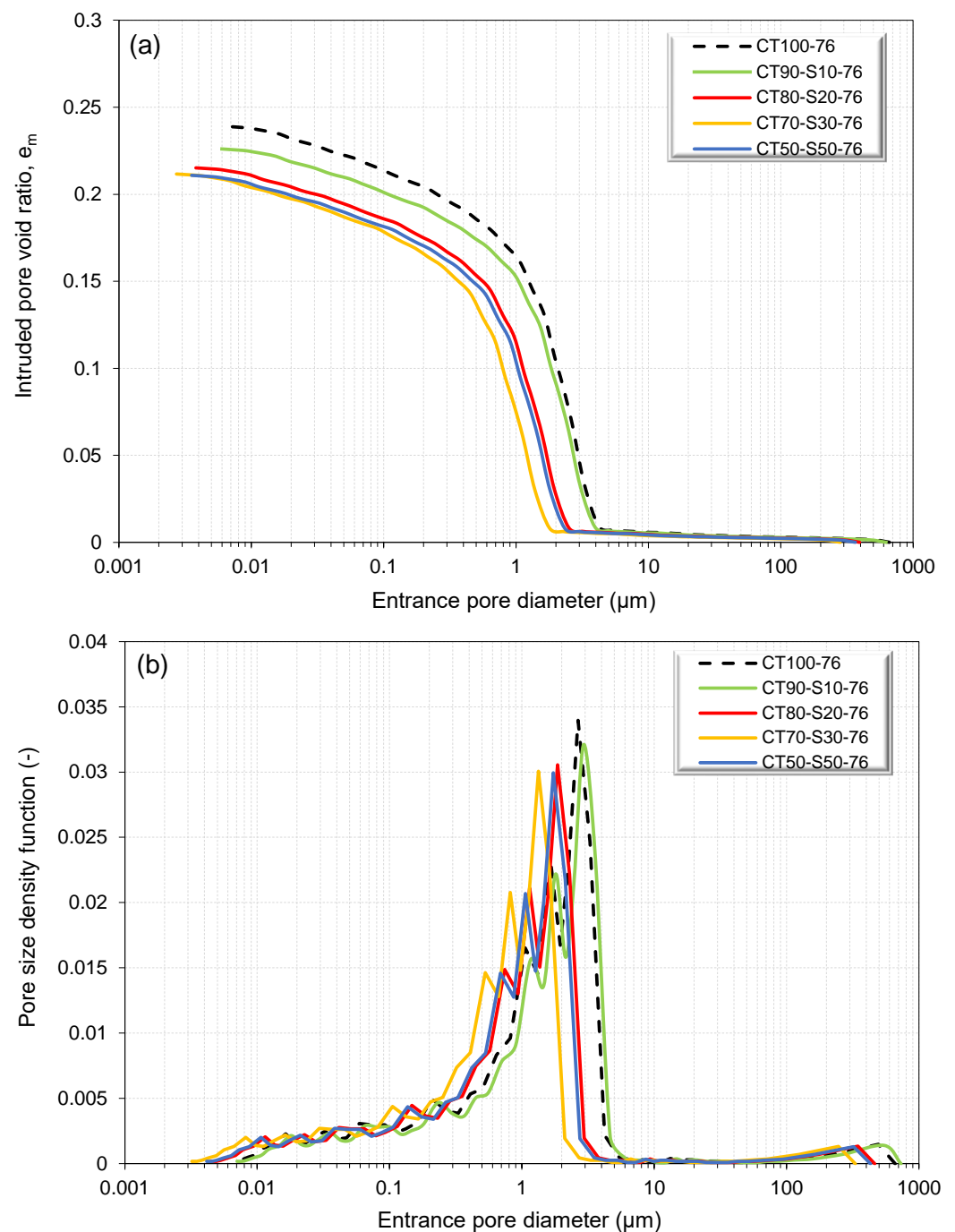


**Figure 6.** MIP results of 76 wt.% solid fill specimens: (a) cumulative; (b) incremental curves.

In addition to the particle size distribution, CaO (55.6%) within sand encourages the hydration products (C-S-H) to appear, contributing to the filling of pores. The hydration products resulted in a significant reduction in pore size and porosity [58–60]. Accordingly, the strength of CPB improved significantly. For example, CT70-S30-72 and CT70-S30-76 samples had lower porosity values (2.84% and 6.72%, respectively) when compared to the control samples. However, one could interpret that CPB's pore size augmented at a 50% sand addition. Note that sand exceeding the threshold limit (30%) caused segregation in CPB. Segregation disrupts the uniformity of backfill mixtures by causing friction and breaking of bonds between the particles [61–63]. This results in an increase in the voids of CPB and the formation of different strength values in different parts of CPB samples.

### 3.4. SEM Observations of CPB Samples

Figures 7 and 8 indicate the SEM-EDS results of 56-day cured filling specimens (C70-S30-72 and C70-S30-76) at different solid contents. The circulation of sand, pores, bonds, and cracks on the outside of the filling specimens studied could be observed easily. In addition, the compact structure that was formed due to the fill's high solid content made CPBs denser. It has been observed that different hydration products are formed as a result of the interaction of sand with tailings. In addition, it has been found that the grains in tailings are glued with hydration materials. However, there are few voids between the grains. It can be interpreted that these gaps are eliminated by well-graded sand.

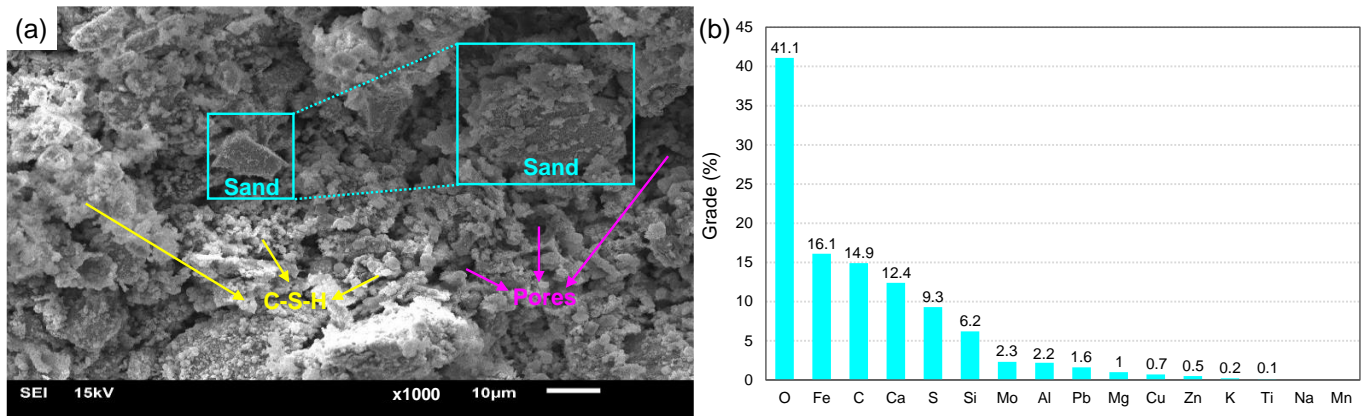


Figure 7. SEM (a) and EDS (b) results of 56-day cured CPB samples with 72 wt.% solid contents.

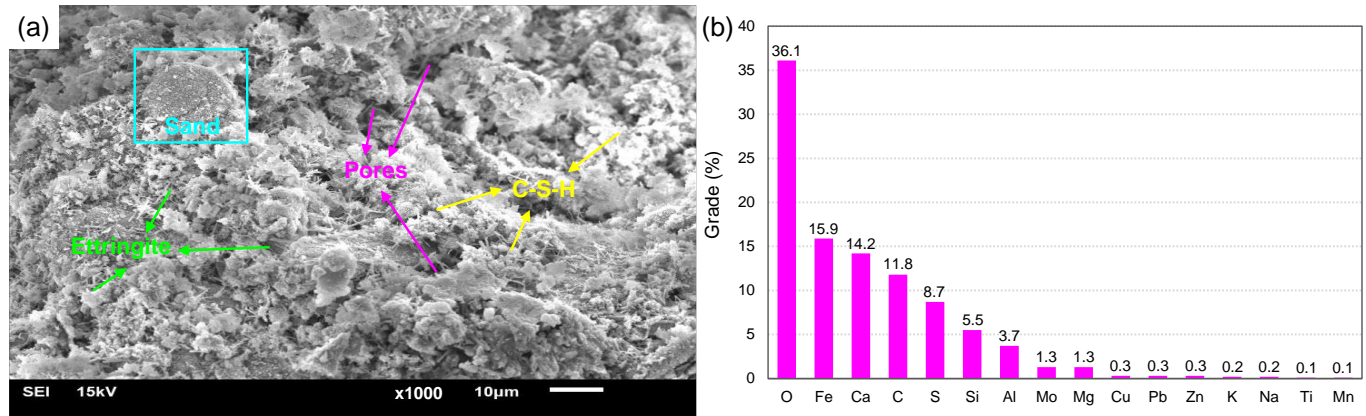


Figure 8. SEM (a) and EDS (b) results of 56-day cured CPB samples with 76 wt.% solid contents.

In addition, different quantities of CSH gels and ettringite bonds were observed in both solid contents. This could be clarified by the amount of Ca contained in the sand [64–66]. According to EDS results, the key features in hydration products of CT70-S30-72 are O, Fe, C, Ca, S, Si, Mo, Al, and Mg with a mass fraction of 41.1%, 16.1%, 14.9%, 12.4%, 9.3%, 6.2%, 2.2%, 1.0%, and 2.3%, respectively. Similarly, the same main elements of CT70-S30-76 are 36.1%, 15.9%, 11.8%, 14.2%, 8.7%, 5.5%, 1.3%, 3.7%, and 1.3%, respectively. The circulation of O, Fe, C, Ca, S, Si, and Al elements is strictly linked to the fill's mineral composition, and it appears to have clear limits in the delivery area. Between these elements, Ca is dispersed in cement and sand hydration products. Si and Al elements occupy a large place on the surface of cement and are usually found in small amounts in CPB [67–69]. The excess content of Ca, Si, O, and Al elements in the hydration materials supports the formation of SiO<sub>2</sub> and Al<sub>2</sub>O<sub>3</sub> in the content of sand and cement and makes a positive contribution to the strengths.

#### 4. Conclusions

The usability of sand in backfill manufacturing was explored experimentally. The mini-slump, UCS, and microstructural (SEM-EDX and MIP) properties of CPB, when produced with different solid contents and tailings/sand ratios, were investigated experimentally. As a result of this lab-scale study, the optimum sand replacement ratio for backfilling was determined in terms of rheology and strength, considering the operational conditions. The key consequences of this research are below:

1. Since the totaling of sand to the backfill increased the mixture gradation, the compressive strengths were found to be greater at up to 89.0% and 99.2% of the solid contents of 72% and 76%, respectively, compared to samples without sand.
2. Increasing the replacement ratio of the sand used within CPB increases the corresponding strength but reduces strength after a threshold limit of 30%, causing segregation.
3. Inert sand with a high CaO ratio can be used as a cement material as well as being used as an aggregate in CPB samples, providing high strengths even at low cement amounts. This shows the importance of using sand to reduce cement costs.

The results of the research show that the use of sand in mixtures improves the mechanical properties of CPB and can reduce cement-related costs depending on the distance of the quarry to the mine. However, using a high amount of sand adversely affects CPB's rheological properties. In addition to the backfill strengths, rheological properties should be also taken into consideration. The gradation of sand should be determined accurately, together with the suitable replacement ratio. In upcoming studies, the writers will ruminate further on the optimization of sand when used as aggregate in CPB with different mineral/chemical additives, as well as some other reinforcement agents. All these works are currently underway.

**Author Contributions:** Conceptualization, N.U.G. and E.Y.; methodology, M.S. and T.K.; writing—original draft preparation, N.U.G.; writing—review and editing, N.U.G., E.Y., M.S. and T.K.; and supervision, E.Y. All authors have read and agreed to the published version of the manuscript.

**Funding:** This research received no external funding.

**Data Availability Statement:** No new data were created or analyzed in this study. Data sharing is not applicable to this article.

**Conflicts of Interest:** The authors declare no conflict of interest.

#### References

1. Gedam, V.V.; Raut, R.D.; de Sousa Jabbour, A.B.L.; Agrawal, N. Moving the circular economy forward in the mining industry: Challenges to closed-loop in an emerging economy. *Resour. Policy* **2021**, *74*, 102279. [[CrossRef](#)]
2. Kasap, T.; Yilmaz, E.; Guner, N.U.; Sari, M. Recycling dam tailings as cemented mine backfill: Mechanical and geotechnical properties. *Adv. Mater. Sci. Eng.* **2022**, *2022*, 6993068. [[CrossRef](#)]
3. Løvik, A.N.; Hagelüken, C.; Wäger, P. Improving supply security of critical metals: Current developments and research in the EU. *Sustain. Mater. Technol.* **2018**, *15*, 9–18. [[CrossRef](#)]
4. Covre, P.W.; Ramos, S.J.; da Silveira Pereira, W.V.; de Souza, E.S.; Martins, G.C.; Teixeira, O.M.M.; Fernandes, A.R. Impact of copper mining wastes in the Amazon Properties and risks to environment and human health. *J. Hazard. Mater.* **2021**, *421*, 126688. [[CrossRef](#)] [[PubMed](#)]
5. Chen, S.; Wang, W.; Yan, R.; Wu, A.; Wang, Y.; Yilmaz, E. A joint experiment and discussion for strength characteristics of cemented paste backfill considering curing conditions. *Minerals* **2022**, *12*, 211. [[CrossRef](#)]
6. Lu, H.; Qi, C.; Chen, Q.; Gan, D.; Xue, Z.; Hu, Y. New procedure for recycling waste tailings as cemented paste backfill to underground stopes and open pits. *J. Clean. Prod.* **2018**, *188*, 601–612. [[CrossRef](#)]
7. Kongar-Syuryun, C.; Ivannikov, A.; Khayrutdinov, A.; Tyulyaeva, Y. Geotechnology using composite materials from man-made waste is a paradigm of sustainable development. *Mater. Today Proc.* **2021**, *38*, 2078–2082. [[CrossRef](#)]
8. Li, J.J.; Yilmaz, E.; Cao, S. Influence of industrial solid waste as filling material on mechanical and microstructural characteristics of cementitious backfills. *Constr. Build. Mater.* **2021**, *299*, 124288. [[CrossRef](#)]
9. Saedi, A.; Jamshidi-Zanjani, A.; Darban, A.K. A review of additives used in the cemented paste tailings: Environmental aspects and application. *J. Environ. Manag.* **2021**, *289*, 112501. [[CrossRef](#)]

10. Zhao, D. Reactive MgO-modified slag-based binders for cemented paste backfill and potential heavy-metal leaching behavior. *Constr. Build. Mater.* **2021**, *298*, 123894. [[CrossRef](#)]
11. Kefeni, K.K.; Msagati, T.A.; Mamba, B.B. Acid mine drainage: Prevention, treatment options, and resource recovery A review. *J. Clean. Prod.* **2017**, *151*, 475–493. [[CrossRef](#)]
12. Hefni, M.; Ahmed, H.A.; Omar, E.S.; Ali, M.A. The potential re-use of Saudi mine tailings in mine backfill: A path towards sustainable mining in Saudi Arabia. *Sustainability* **2021**, *13*, 6204. [[CrossRef](#)]
13. Li, J.J.; Cao, S.; Yilmaz, E.; Liu, Y.P. Compressive fatigue behavior and failure evolution of additive fiber-reinforced cemented tailings composites. *Int. J. Miner. Metall. Mater.* **2022**, *29*, 345–355. [[CrossRef](#)]
14. Behera, S.K.; Ghosh, C.N.; Mishra, D.P.; Singh, P.; Mishra, K.; Buragohain, J.; Mandal, P.K. Strength development and microstructural investigation of lead-zinc mill tailings based paste backfill with fly ash as alternative binder. *Cem. Concr. Compos.* **2020**, *109*, 103553. [[CrossRef](#)]
15. Yilmaz, E.; Belem, T.; Benzaazoua, M. One-dimensional consolidation parameters of cemented paste backfills. *Gospod. Surowcamii Miner. / Miner. Resour. Manag.* **2012**, *28*, 29–45.
16. Qi, C.; Fourie, A. Cemented paste backfill for mineral tailings management: Review and future perspectives. *Miner. Eng.* **2019**, *144*, 106025. [[CrossRef](#)]
17. Xue, G.L.; Yilmaz, E.; Feng, G.R.; Cao, S.; Sun, L.J. Reinforcement effect of polypropylene fiber on dynamic properties of cemented tailings backfill under SHPB impact loading. *Constr. Build. Mater.* **2021**, *279*, 122417. [[CrossRef](#)]
18. Bull, A.J.; Fall, M. Thermally induced changes in metalloid leachability of cemented paste backfill that contains blast furnace slag. *Miner. Eng.* **2020**, *156*, 106520. [[CrossRef](#)]
19. Huang, Z.; Yilmaz, E.; Cao, S. Analysis of strength and microstructural characteristics of mine backfills containing fly ash and desulfurized gypsum. *Minerals* **2021**, *11*, 409. [[CrossRef](#)]
20. Koohestani, B.; Koubaa, A.; Belem, T.; Bussi re, B.; Bouzahzah, H. Experimental investigation of mechanical and microstructural properties of cemented paste backfill containing maple-wood filler. *Constr. Build. Mater.* **2016**, *121*, 222–228. [[CrossRef](#)]
21. Yang, L.; Wang, H.; Wu, A.; Li, H.; Bruno, T.A.; Zhou, X.; Wang, X. Effect of mixing time on hydration kinetics and mechanical property of cemented paste backfill. *Constr. Build. Mater.* **2020**, *247*, 118516. [[CrossRef](#)]
22. Ermolovich, E.A.; Ivannikov, A.L.; Khayrutdinov, M.M.; Kongar-Syuryun, C.B.; Tyulyaeva, Y.S. Creation of a nanomodified backfill based on the waste from enrichment of water-soluble ores. *Materials* **2022**, *15*, 3689. [[CrossRef](#)] [[PubMed](#)]
23. Li, J.J.; Yilmaz, E.; Cao, S. Influence of solid content, cement/tailings ratio, and curing time on rheology and strength of cemented tailings backfill. *Minerals* **2020**, *10*, 922. [[CrossRef](#)]
24. Pan, A.; Grabinsky, M. Mechanical characterization of cemented paste backfill. *Eng* **2023**, *4*, 738–747. [[CrossRef](#)]
25. Liu, Q.; Liu, D.; Tian, Y.; Liu, X. Numerical simulation of stress-strain behaviour of cemented paste backfill in triaxial compression. *Eng. Geol.* **2017**, *231*, 165–175. [[CrossRef](#)]
26. Mangane, M.B.C.; Argane, R.; Trauchessec, R.; Lecomte, A.; Benzaazoua, M. Influence of superplasticizers on mechanical properties and workability of cemented paste backfill. *Miner. Eng.* **2018**, *116*, 3–14. [[CrossRef](#)]
27. Deng, X.; Zhang, J.; Klein, B.; Zhou, N.; Dewit, B. Experimental characterization of the influence of solid components on the rheological and mechanical properties of cemented paste backfill. *Int. J. Miner. Process.* **2017**, *168*, 116–125. [[CrossRef](#)]
28. Xue, X.; Gu, Y.; Zhang, X.; Wu, S.; Sun, P.; Cui, J.; Wang, X. Mechanical behavior and microscopic mechanism of fiber reinforced coarse aggregate cemented backfill. *Constr. Build. Mater.* **2023**, *366*, 130093. [[CrossRef](#)]
29. Kasap, T.; Yilmaz, E.; Sari, M. Effects of mineral additives and age on microstructure evolution and durability properties of sand-reinforced cementitious mine backfills. *Constr. Build. Mater.* **2022**, *352*, 129079. [[CrossRef](#)]
30. Lyu, H.; Chen, Y.; Pu, H.; Ju, F.; Zhang, K.; Li, Q.; Wu, P. Dynamic properties and fragmentation mechanism of cemented tailings backfill with various particle size distributions of aggregates. *Constr. Build. Mater.* **2023**, *366*, 130084. [[CrossRef](#)]
31. Koohestani, B.; Mokhtari, P.; Yilmaz, E.; Mahdipour, F.; Darban, A.K. Geopolymerization mechanism of binder-free mine tailings by sodium silicate. *Constr. Build. Mater.* **2021**, *268*, 121217. [[CrossRef](#)]
32. Ueno, A.; Ogawa, Y. Influence of coarse aggregate shape on optimum fine to total aggregate ratio using a virtual voids-ratio diagram in concrete compaction. *Cem. Concr. Compos.* **2020**, *106*, 103463. [[CrossRef](#)]
33. Ji, X.; Gu, X.; Wang, Z.; Xu, S.; Jiang, H.; Yilmaz, E. Admixture effects on the rheological/mechanical behavior and micro-structure evolution of alkali-activated slag backfills. *Minerals* **2023**, *13*, 30. [[CrossRef](#)]
34. Li, L.; Zhan, B.J.; Lu, J.; Poon, C.S. Systematic evaluation of the effect of replacing river sand by different particle size ranges of fine recycled concrete aggregates (FRCA) in cement mortars. *Constr. Build. Mater.* **2019**, *209*, 147–155. [[CrossRef](#)]
35. Kumar, S.P.; Balasubramanian, M. Mechanical and micro structure analysis on river sand replaced with quarry dust in self-compacting concrete. *Mater. Today Proc.* **2022**, *68*, 2413–2420. [[CrossRef](#)]
36. Sari, M.; Yilmaz, E.; Kasap, T.; Karasu, S. Exploring the link between ultrasonic and strength behavior of cementitious mine backfill by considering pore structure. *Constr. Build. Mater.* **2023**, *370*, 130588. [[CrossRef](#)]
37. Cheng, A.; Shu, P.; Deng, D.; Zhou, C.; Huang, S.; Ye, Z. Microscopic acoustic emission simulation and fracture mechanism of cemented tailings backfill based on moment tensor theory. *Constr. Build. Mater.* **2021**, *308*, 125069. [[CrossRef](#)]
38. Zhao, K.; Yu, X.; Zhu, S.; Zhou, Y.; Wang, Q.; Wang, J. Acoustic emission investigation of cemented paste backfill prepared with tantalum-niobium tailings. *Constr. Build. Mater.* **2020**, *237*, 117523. [[CrossRef](#)]

39. Gao, S.; Li, W.; Yuan, K.; Rong, C. Properties and application of thixotropic cement paste backfill with molybdenum tailings. *J. Clean. Prod.* **2023**, *391*, 136169. [[CrossRef](#)]
40. Ouattara, D.; Yahia, A.; Mbonimpa, M.; Belem, T. Effects of superplasticizer on rheological properties of cemented paste backfills. *Int. J. Miner. Process.* **2017**, *161*, 28–40. [[CrossRef](#)]
41. Gao, B.; Cao, S.; Yilmaz, E. Effect of content and length of polypropylene fibers on strength and microstructure of cementitious tailings-waste rock fill. *Minerals* **2023**, *13*, 142. [[CrossRef](#)]
42. Zhou, N.; Zhang, J.; Ouyang, S.; Deng, X.; Dong, C.; Du, E. Feasibility study and performance optimization of sand-based cemented paste backfill materials. *J. Clean. Prod.* **2020**, *259*, 120798. [[CrossRef](#)]
43. Kasap, T.; Yilmaz, E.; Sari, M. Physico-chemical and micro-structural behavior of cemented mine backfill: Effect of pH in dam tailings. *J. Environ. Manage.* **2022**, *314*, 115034. [[CrossRef](#)]
44. Yang, X.; Xiao, B.; Gao, Q.; He, J. Determining the pressure drop of cemented Gobi sand and tailings paste backfill in a pipe flow. *Constr. Build. Mater.* **2020**, *255*, 119371. [[CrossRef](#)]
45. Zhou, N.; Du, E.; Zhang, J.; Zhu, C.; Zhou, H. Mechanical properties improvement of sand-based cemented backfill body by adding glass fibers of different lengths and ratios. *Constr. Build. Mater.* **2021**, *280*, 122408. [[CrossRef](#)]
46. Sun, Q.; Zhang, J.; Zhou, N. Early-age strength of aeolian sand-based cemented backfilling materials: Experimental results. *Arab. J. Sci. Eng.* **2018**, *43*, 1697–1708. [[CrossRef](#)]
47. Deng, D.Q.; Liang, Y.H.; Huangfu, F.C. Properties of Gobi aggregate and sulfide-rich tailings cemented paste backfill and its application in a high-stress metal mine. *Adv. Civ. Eng.* **2021**, *2021*, 6624915. [[CrossRef](#)]
48. Ouyang, S.; Huang, Y.; Zhou, N.; Li, J.; Gao, H.; Guo, Y. Experiment on hydration exothermic characteristics and hydration mechanism of sand-based cemented paste backfill materials. *Constr. Build. Mater.* **2022**, *318*, 125870. [[CrossRef](#)]
49. Solismaa, S.; Torppa, A.; Kuva, J.; Heikkilä, P.; Hyvönen, S.; Juntunen, P.; Benzaazoua, M.; Kauppila, T. Substitution of cement with granulated blast furnace slag in cemented paste backfill: Evaluation of technical and chemical properties. *Minerals* **2021**, *11*, 1068. [[CrossRef](#)]
50. Sari, M.; Yilmaz, E.; Kasap, T.; Guner, N.U. Strength and microstructure evolution in cemented mine backfill with low and high pH pyritic tailings: Effect of mineral admixtures. *Constr. Build. Mater.* **2022**, *328*, 127109. [[CrossRef](#)]
51. Jia, Q.; Yang, Q.; Guo, L.; Knutsson, S.; Xue, P.; Liu, G.; Jiang, L. Effects of fine content, binder type and porosity on mechanical properties of cemented paste backfill with co-deposition of tailings sand and smelter slag. *Electron. J. Geotech. Eng.* **2016**, *21*, 6971–6988.
52. Malusis, M.A.; Evans, J.C.; McLane, M.H.; Woodward, N.R. A miniature cone for measuring the slump of soil-bentonite cutoff wall backfill. *Geotech. Test. J.* **2008**, *31*, 373–380.
53. Chen, S.; Yilmaz, E.; Xiang, Z.; Wang, Y. Curing conditions effect on pore structure, compressive strength and elastic modulus of cementitious tailings backfills. *Powder Technol.* **2023**, *in press*. [[CrossRef](#)]
54. Chen, Q.; Tao, Y.; Feng, Y.; Zhang, Q.; Liu, Y. Utilization of modified copper slag activated by Na<sub>2</sub>SO<sub>4</sub> and CaO for unclassified lead/zinc mine tailings based cemented paste backfill. *J. Environ. Manage.* **2021**, *290*, 112608. [[CrossRef](#)]
55. Vargas, F.; Alsina, M.A.; Gaillard, J.F.; Pasten, P.; Lopez, M. Copper entrapment and immobilization during cement hydration in concrete mixtures containing copper tailings. *J. Clean. Prod.* **2021**, *312*, 127547. [[CrossRef](#)]
56. Xue, G.L.; Yilmaz, E. Strength, acoustic, and fractal behavior of fiber reinforced cemented tailings backfill subjected to triaxial compression loads. *Constr. Build. Mater.* **2022**, *338*, 127667. [[CrossRef](#)]
57. Liu, S.G.; Fall, M. Fresh and hardened properties of cemented paste backfill: Links to mixing time. *Constr. Build. Mater.* **2022**, *324*, 126688. [[CrossRef](#)]
58. Wang, Y.; Duc, M.; Cui, Y.J.; Tang, A.M.; Benahmed, N.; Sun, W.J.; Ye, W.M. Aggregate size effect on the development of cementitious compounds in a lime-treated soil during curing. *Appl. Clay Sci.* **2017**, *136*, 58–66. [[CrossRef](#)]
59. Dixit, A.; Patel, A.S.; Singh, D. Effect of different supplementary cementitious materials on compressive strength of concrete with varying size of aggregates. *Mater. Today Proc.* **2022**, *56*, 336–341. [[CrossRef](#)]
60. Ying, Z.; Cui, Y.J.; Benahmed, N.; Duc, M. Changes in microstructure and water retention property of a lime-treated saline soil during curing. *Acta Geotech.* **2022**, *17*, 319–326. [[CrossRef](#)]
61. Tian, X.; Fall, M. Non-isothermal evolution of mechanical properties, pore structure and self-desiccation of cemented paste backfill. *Constr. Build. Mater.* **2021**, *297*, 123657. [[CrossRef](#)]
62. Wang, Z.; Qi, T.; Feng, G.; Bai, J.; Pei, X.; Cui, B.; Song, C.; Ran, H. Electrical resistivity method to appraise static segregation of gangue-cemented paste backfill in the pipeline. *Int. J. Press. Vessel. Pip.* **2021**, *192*, 104385. [[CrossRef](#)]
63. Wang, Z.; Feng, G.; Qi, T.; Guo, Y.; Du, X. Evaluation of static segregation of cemented gangue-fly ash backfill material using electrical resistivity method. *Measurement* **2020**, *154*, 107483. [[CrossRef](#)]
64. Béket Dalcé, J.; Li, L.; Yang, P. Experimental study of uniaxial compressive strength (UCS) distribution of hydraulic backfill associated with segregation. *Minerals* **2019**, *9*, 147. [[CrossRef](#)]
65. Benkirane, O.; Haruna, S.; Fall, M. Strength and microstructure of cemented paste backfill modified with nano-silica particles and cured under non-isothermal conditions. *Powder Technol.* **2023**, *419*, 118311. [[CrossRef](#)]
66. Wang, Y.; Cao, Y.; Zhang, Z.; Zhang, P.; Ma, Y.; Wang, A.; Wang, H. Intrinsic sulfuric acid resistance of C-(N)-ASH and NASH gels produced by alkali-activation of synthetic calcium aluminosilicate precursors. *Cem. Concr. Res.* **2023**, *165*, 107068. [[CrossRef](#)]

67. Sari, M.; Yilmaz, E.; Kasap, T. Long-term ageing characteristics of cemented paste backfill: Usability of sand as a partial substitute of hazardous tailings. *J. Clean. Prod.* **2023**, *401*, 136723. [[CrossRef](#)]
68. Cao, S.; Xue, G.L.; Yilmaz, E. Flexural behavior of fiber reinforced cemented tailings backfill under three-point bending. *IEEE Access* **2019**, *7*, 139317–139328. [[CrossRef](#)]
69. Jiang, H.; Han, J.; Ren, L.; Guo, Z.; Yilmaz, E. Study of early-age performance of cementitious backfills with alkali activated slag under internal sulfate attack. *Constr. Build. Mater.* **2023**, *372*, 130786. [[CrossRef](#)]

**Disclaimer/Publisher's Note:** The statements, opinions and data contained in all publications are solely those of the individual author(s) and contributor(s) and not of MDPI and/or the editor(s). MDPI and/or the editor(s) disclaim responsibility for any injury to people or property resulting from any ideas, methods, instructions or products referred to in the content.